Photocatalytic NO_x abatement by calcium aluminate cements modified with TiO_2: improved NO_2 conversion

M. Pérez-Nicolás[a], J. Balbuena[b] M. Cruz-Yusta[b], L. Sánchez[b], I. Navarro-Blasco[a], J.M. Fernández[a], J.I. Alvarez[a]*

[a] *MIMED Research Group, Department of Chemistry and Soil Sciences, School of Sciences, University of Navarra. c/ Irunlarrea, 1. 31008 Pamplona, Spain*
[b] *Department of Inorganic Chemistry, School of Sciences, University of Córdoba, Campus de Rabanales, Edificio Marie Curie, 14071 Córdoba, Spain*

Keywords: D: Calcium Aluminate Cement; B: X-ray Diffraction; B: EDX; C: Compressive Strength; NOx abatement

Abstract

Photocatalytic activity of TiO_2 was studied in two types of Calcium Aluminate Cement (CAC) under two different curing regimes. The effect of the TiO_2 addition on the setting time, consistency and mechanical properties of the CACs was evaluated. The abatement of gaseous pollutants (NO_x) under UV irradiation was also assessed. These cementitious matrices were found to successfully retain NO_2: more abundant presence of aluminates in white cement (w-CAC, iron-lean) helped to better adsorb NO_2, thus improving the conversion performance of the catalyst resulting in a larger NO_x removal under UV irradiation. As evidenced by XRD, SEM, EDAX and zeta potential analyses, the presence of ferrite in dark cement (d-CAC, iron-reach) induced a certain chemical interaction with TiO_2. The experimental findings suggest the formation of new iron titanate phases, namely pseudobrookite. The reduced band-gap energy of these compounds compared with that of TiO_2 accounts for the photocatalytic activity of these samples.

*Corresponding author:
Dr. José Ignacio Alvarez
Dpto. de Química y Edafología
Facultad de Ciencias, Universidad de Navarra
C/ Irunlarrea, 1, 31.008 Pamplona (Navarra), Spain
Phone: 34 948 425600; Fax: 34 948 425670
e-mail: jalvarez@unav.es; mimed@unav.es

1. Introduction

The atmospheric pollution caused by the presence in the air of nitrogen oxides, NO_x, has been recognised as one of the most serious environmental problems [1]. In the urban atmosphere NO_x are one of the most common gaseous pollutants being very harmful to the human health. Their release towards the earth atmosphere causes adverse environmental effects (like acid rain and ozone depletion) [2]. Accordingly, the finding of ways to promote the NO_x removal from the atmosphere is important. The use of photochemical oxidation (PCO) assisted processes has gained a great attention to facilitate the degradation of inorganic toxic gases and organic pollutants, the main focus being so far placed - although not only- on the use of TiO_2 and the combinations thereof [3].

To improve practical applications, the powdered photocatalysts should be immobilized to provide surfaces that can be reached by light irradiation. Binding materials are useful to this aim, under condition that (i) allow photocatalyst particles to act, presenting low degree of chemical interaction with them; (ii) show stability in the face of products formed after the photocatalytic reaction; (iii) provide enough surface area to ensure a good level of photocatalytic reaction; and (iv) are environmentally friendly.

For example, these photocatalytic agents have been successfully included in Portland Cement (PC) originating improved materials not only with depolluting properties but also with self-cleaning ability of their surfaces [4,5]. The incorporation of photocatalysts into cement-based materials guarantees a widespread distribution of the active agent and, if applied to enough outdoor exposed surfaces, could be helpful to reduce the contaminants level, especially in urban environments. On the other hand, the self-cleaning capacity safeguards the aesthetic characteristics and at the same time minimizes the maintenance and cleaning expenses [6].

The PCO of NO_X occurs through the following reactions [7]:

$$TiO_2 + h\nu \rightarrow e^- + h^+ \quad (1)$$

$$H_2O + h^+ \rightarrow H^+ + OH\bullet \quad (2)$$

$$O_2 + e^- \rightarrow O_2\bullet^- \quad (3)$$

$$NO + O_2\bullet^- \rightarrow NO_3^- \quad (4)$$

$$NO + OH\bullet \rightarrow HNO_2 \quad (5)$$

$$HNO_2 + OH\bullet \rightarrow NO_2 + H_2O \quad (6)$$

$$NO_2 + OH\bullet \rightarrow NO_3^- + H^+ \quad (7)$$

Even though the NO_x is mainly captured on surface in the form of alkaline nitrate (reaction 7), the acids formation (reactions 5 and 7), has been reported to cause a certain degree of erosion of the PC-based mortars (by acid-base reaction) [8]. Besides, certain amounts of NO_2 – produced in the photocatalytic process (reaction 6) – have been reported to be evolved and unretained by the PC systems. These amounts of released NO_2 partially counteract the photocatalytic efficiency [7,9,10].

Calcium aluminate cement (CAC) is another type of cement with specific characteristics, primarily made of monocalcium aluminate (CA), together with different proportions of $C_{12}A_7$, C_5A_3, C_3A and C_4AF. The hydration of this type of cement takes place yielding metastable hydrated compounds, such as the hexagonal phases, $CaAl_2O_4\bullet10H_2O$ (CAH_{10}) and $Ca_2Al_2O_5\bullet8H_2O$ (C_2AH_8) and amorphous aluminium hydroxide. Metastable phases will spontaneously be converted into stable compounds but this conversion can also be accelerated under conditions of higher temperature and relative humidity. The stable cubic phases formed are mainly hydrogarnet $Ca_3Al_2O_6\bullet6H_2O$ (C_3AH_6) and crystalline $Al_2O_3\bullet3H_2O$ (AH_3) [11]. The composition of these CACs confers interesting properties such as rapid strength gain, enhanced resistance to extreme temperatures, abrasion, acid corrosion, sulfate attack and alkali-silica reaction [12]. CACs are gaining interest due to their rapid hardening and enhanced durability properties as compared with other cements [13,14].

Although CAC is used in many building as well as industrial structures, its modification upon addition of photocatalytic additives has not yet been addressed and that is precisely the purpose of the present work. We intend to obtain for the first time depolluting CAC mortars modified with different amounts of TiO_2. The effect of the TiO_2 incorporation on setting time, compressive strength and mineralogical composition of the CAC mortars will be assessed. PCO efficiency of these TiO_2-bearing CAC mortars will be also measured by means of the NO_x abatement. The modified depolluting mortars could be then applied in different tunnels, industrial floors and urban areas in which CACs are usually applied.

2. Experimental section

2.1. Materials

Two different CACs were used to prepare the mortars: one was an iron-rich (17 wt.% content in Fe_2O_3, as mineralogical phase of ferrite, Ca_2FeAlO_5, C_4AF), dark cement (d-CAC) and the other was an iron-lean (0.1 wt.% content in Fe_2O_3), white cement (w-CAC), supplied by Ciments Molins and Kerneos, respectively (chemical and mineralogical compositions provided in Table 1). A siliceous aggregate was also used [15]. As photocatalyst, TiO_2 (Aeroxide P25, Evonik; average particle size: 21 nm; surface area 50±15 m^2g^{-1}) composed of 75% anatase and 25% rutile was used. A polycarboxylate-based superplasticizer (Melflux2651^e, BASF) was also incorporated to ensure a good workability of the mortars.

2.2. Methods

Mortar preparation and curing regimes

Samples were prepared with a cement:aggregate ratio of 1:3 by weight (with cement:water 1:0.37). Different amounts of TiO_2 were added: 1%, 3%, 5% and 10 wt.% with respect to the cement. These samples required different amounts of superplasticizer (Table 2) that were

used to prepare samples that yielded a mortar slump of 175±10 mm, according to the flow table test [16].

Cement, aggregate and additives were blended for 10 min at low speed in a mixer. Water was then added and mixed for 90 s at low speed. Then, fresh state properties were determined as described below. Afterwards, mortars were moulded in 36x40 mm cylindrical casts and de-moulded 24 h later. Half of the moulds were cured at 20°C and 95% RH (curing condition 1), and the other half were initially cured at 60°C and 100% RH for 24 h; later, temperature and RH were shifted towards 20°C and 95% RH (curing condition 2). Under the curing condition 1, CAC mortars should develop metastable hydrated phases, whereas the second curing regime was applied in order to enhance the formation of stable cubic aluminate hydrates [15].Samples were cured for 28 days. Three specimens of each mortar were tested at each curing time in order to make results representative.

Mortars characterization and properties

In the fresh state, consistency (measured by means of the flow table test [16]) and setting time [17] were assessed. In pastes, surface charge of the cement particles upon increasing amounts of TiO_2 was measured by the zeta potential values (Colloidal Dynamics Zeta-Probe) with an automatic titrator. Pastes of the two types of cement (d-CAC and w-CAC) were prepared (25 g of cement and 150 mL of deionized water) and titrated with a 0.5 wt.% TiO_2 aqueous suspension. The zeta potential of the titrant suspension was obtained as a reference.

After 28 curing days, in hardened samples, compressive strengths were measured at a loading rate of 50 $N \cdot s^{-1}$. Pore size distributions (PSD) were obtained by mercury intrusion porosimetry (Micromeritics-AutoPoreIV-9500; pressure 0.0015 to 207 MPa). Mineralogical characterization by X-ray diffraction (XRD) was done in a Bruker D8 ($CuK_{\alpha 1}$, from 2º to 80º 2θ; increment of 0.02º at 1 $step.s^{-1}$ scan rate).

Textural characteristics and elemental compositions of the samples were performed by a Zeiss DSM-940A SEM coupled with an EDAX probe.

Photocatalytic studies: NO_x oxidation

NO_x oxidation tests were done on mortars in a laminar-flow reactor (ISO 22197-1 [18]) and irradiated with a xenon lamp (Solarbox 3000), with an irradiance of 25±1 $W \cdot m^{-2}$, adjusted by a Delta-Ohm HD-2101.1 photoradiometer, with a LP-471 probe (315-400 nm). Conditions were 50±10% RH and 25±2ºC. The photoreactor (300 mL) was fed by a 1000 ppb NO stream. The residence time of NO in the photoreactor was ca. 4 s. Concentrations of NO and NO_2 were determined by chemiluminescence (Environnement AC32M) at a 3.0 $L \cdot min^{-1}$ flow.

NO_x stream flowed over the sample in the dark for 10 min. Then, the photoreactor was irradiated for 30 min. Neither NO_x adsorption on mortar surface nor direct photolysis evidences were found.

3. Results and discussion

3.1. Effect of the TiO_2 on the properties of CAC mortars

The incorporation of the photocatalytic additive gave rise to an increase in water demand owing to the small particle size of the TiO_2. The higher the amount of photocatalyst, the larger was the percentage of superplasticizer (Table 2).

Incorporation of TiO_2 resulted in a slight setting time delay, as can be seen in data collected in Table 2: plain CAC samples showed a setting time of 15 min (d-CAC) or 5 min (w-CAC), whereas 3 wt.% TiO_2-bearing d-CAC and w-CAC samples showed setting times of 26 and 20 min, respectively. As it is well known, the presence of significant amounts of superplasticizer

in the fresh mixtures contributed to the delay in the setting time [19]. The iron-lean CAC (white cement) offered the shortest setting times in comparison with the iron-rich CAC (dark cement). This fact can also be ascribed to the faster hydration of calcium aluminates as compared with the hydration of the ferrite phase ($Ca_2(Al_xFe_{1-x})_2O_5$) [20], which is the main distinguishing cementitious phase that is present in large amount in the dark, iron-rich cement [21]. Ferrite includes a wide range of solid solutions with the aforementioned general formula. Owing to the clinker composition, this phase appears in the iron-rich CAC while it is absent in iron-lean CAC. In spite of the long-term reactivity of the ferrite, its hydration has been described as almost negligible at ambient temperatures (ca. 20ºC) [14].

To summarize, given that the two CACs are quick setting cements with short setting times (as compared with PC that usually shows a setting time of ca. 180 min [22]), the induced delays did not involve significantly negative consequences for their practical application.

Incorporation of TiO_2 yielded compressive strengths greater than 20 MPa for all samples (Fig. 1), offering enough mechanical resistance for practical applications. Compressive strengths after curing condition 2 were usually lower than those measured after curing condition 1 (Fig. 1). This fact is related to the conversion reaction that samples underwent under the mild hydrothermal curing condition 2, which originated cubic stable and denser hydrates (mainly hydrogarnet, C_3AH_6, and gibbsite, AH_3) that caused a porosity increase and a subsequent resistance decrease.

This effect was demonstrated by PSD and XRD examinations. An increase in porosity and pore size was seen after the curing condition 2 (Fig. 2). Total porosity values were 10.5% and 14.7% for plain samples after curing conditions 1 and 2, with a mean pore diameter of 0.287 and 0.385 μm, respectively. Metastable compounds (CAH_{10} and C_2AH_8) together with some remaining anhydrous compounds (CA and $C_{12}A_7$ –mayenite-) were seen by XRD of samples under condition 1. After curing condition 2, diffraction peaks of stable aluminate hydrates, hydrogarnet (C_3AH_6) and gibssite (AH_3), were identified (Table 3).

Under curing condition 1, the plain w-CAC sample yielded higher mechanical resistance (47 MPa) than the d-CAC sample (35 MPa). This finding can be due to the larger amount of calcium aluminates of w-CAC (70.9 wt.% content of Al_2O_3 and 28.0 wt.% of CaO) as compared with the lower one of d-CAC (42.0 wt.% content of Al_2O_3 and 37.8 wt.% of CaO), which showed an outstanding amount of ferrite (Table 1). The hydration of calcium aluminates is the main responsible for the early mechanical resistance, whereas there is no significant contribution of the ferrite to the strength in samples cured at ambient conditions, due to its low short-term hydration, as previously mentioned [14].

A detailed and comparative examination of the XRD patterns of 10 wt.% TiO_2 samples was carried out and collected in Table 3. As the intensities of the peaks showed, in general, low signal/noise ratio, XRD profiles obtained on cement pastes (prepared without aggregate) were recorded in order to increase the weight percentage of the formed compounds (Fig. 3).

The relatively low proportion of TiO_2 incorporated to CAC mortars together with the inherent limits of the XRD technique hindered a more precise identification of the peaks. However, some hints regarding the mineralogical phases can be drawn from a careful observation of the XRD results:

(i) for w-CAC mortars, the addition of TiO_2 only led to the observation of anatase peaks (especially its main peak at 25.3º 2θ). This fact suggests the absence of any chemical interaction between TiO_2 and the components of the w-CAC cement.

(ii) Conversely, for d-CAC mortars, the addition of TiO_2 did not result in the clear identification of the anatase peaks. Two magnifications in Fig. 3, corresponding to the main peak of the anatase (25.3º 2θ) and other peaks around 38º 2θ showed that, in spite of the TiO_2 addition, in d-CAC the peaks of the anatase were of very low intensity.

(iii) According to Table 1, ferrite (brownmillerite) is the only distinguishing phase between d-CAC and w-CAC cements. In the TiO_2-free d-CAC sample, the peaks of the brownmillerite

were identified, whereas when TiO_2 was added, these peaks disappeared (see comparative magnification around 34º 2θ in Fig. 3).

(iv) When TiO_2 was added to d-CAC mortars, the scarce intensity of the TiO_2 diffraction peaks (anatase) as well as the disappearance of the ferrite signals suggests that in the iron-rich CAC the TiO_2 added underwent a partial interaction with the ferrite phase that modified its crystallinity and/or even its mineralogical composition. In these samples small diffraction peaks at 17.9, 18.2, 25.6, 32.8, 36.6 and 37.4º 2θ were found. These peaks could be ascribed to the appearance of pseudobrookite (Fe_2TiO_5). In addition, weak diffraction peaks at 32.4, 35.1, 48.8 and 24.0º 2θ could be related to the presence of traces of ilmenite ($FeTiO_3$). The formation of this mixture of iron titanates would be a consequence of the interaction between TiO_2 and ferrite of the d-CAC. The substitution of Ti^{4+} by Fe^{3+} was favoured in our experimental conditions thanks to the closeness of their respective ionic radii (0.64 and 0.67 Å) [23]. The heat evolved during the CAC hydration [24] favoured this hydrothermal system that likely led to the interaction. In this line, several works had reported the obtaining of iron titanates (namely pseudobrookite and ilmenite) by means of low temperature hydrothermal and sol-gel methods [25-27].

The zeta potential assays also confirmed the aforementioned interaction. First of all, the influence of the pH on the zeta potential of an aqueous dispersion of pure TiO_2 must be taken into account. The pH at which the pH of the titania surface is neutral is the isoelectric point (IEP), which is estimated to be around 6.2. At alkaline pH (above the IEP), the –OH groups on the titania surface are deprotonated resulting in negative surface charge (negative zeta potential), with values around -4 mV or even more negative. These data appear reported elsewhere [28].

In the present work, electroacoustic-based zeta potential measurements carried out for both types of CACs, by progressive additions of TiO_2 (Fig. 4), showed different modifications of the original CACs surface charge values. The results for d-CAC, with a continuous increase

towards more positive values, indicated the formation of a new phase, strongly sheltered by positive calcium counterions. Opposite behaviour was found for w-CAC, in which the decrease in zeta potential suggests the absence of interaction, because in the resulting electroacoustic signal, the more positive values (from CAC compounds) were counterbalanced by the negative ones (from TiO_2), without forming a new phase with different surface charge.

As for Portland cement matrices, literature had reported some controversial discussions, in which there was not a clear conclusion on whether the TiO_2 reacted or not with any of the phases of the PC, particularly calcium hydroxide, in a pozzolanic-type reaction [9,29]. However, our experimental evidences for d-CAC helped us to establish a clear interaction TiO_2-ferrite. Further confirmation of this interaction will be provided by SEM-EDAX examination below.

The micrographs of CACs samples under curing condition 1 can be seen in Fig. 5 (d-CAC samples Fig. 5a-d and w-CAC samples Fig. 5e-h). Plain d-CAC as well as w-CAC samples present similar textural appearance (Fig. 5a and 5e), with cracked surfaces and with several well identified compounds, such as hexagonal plate-like crystals of C_2AH_8 metastable calcium aluminates [30] (Fig. 5b), in good agreement with the XRD results. On the other hand, this kind of plate-like crystals can be seen for the plain w-CAC samples accompanied, in a specific area, by spherulite shaped aluminate hydrates (Fig. 5f) [31].

The addition of 5 wt.% of TiO_2 resulted in a different micro-morphology depending on the type of cement: irregular and non-geometric aspect was seen for d-CAC, with some ill-defined clusters, after curing regime 1 (Fig. 5c and Fig. 5d). EDAX analysis of several spots of these samples revealed an expected, predominant composition of calcium aluminates. At the same time, when Ti was identified (see Fig. 5i, as an example), in the analysis carried out in the very same spot, Fe also appeared, in good agreement with the identification of iron titanates by XRD analysis. However, SEM observations for the w-CAC samples allowed us

to see prismatic crystals some of them with rounded edges, with well-defined structures covering the main part of the sample (Fig. 5g and 5h).

From these experimental findings it can be concluded that TiO_2 added into d-CAC gave rise to a heterogeneous matrix, as a result of the TiO_2-ferrite interaction. On the other hand, a physical entrapment – without significant chemical interaction – can be suggested as the main immobilization mechanism of the TiO_2 in w-CAC. In this latter case, the TiO_2 addition remained mainly unaltered within the w-CAC matrix and almost fully available for the photocatalytic processes.

3.2. Assessment of the photocatalytic efficiency

The profiles of NO, NO_2 and NO_x abatement measurements over time are depicted in Fig. 6a and 6b for d-CAC and w-CAC samples, respectively. The NO (and in parallel NO_x) profiles are characterised by three common stages: i) in the absence of UV radiation, neither the activation of the sites of TiO_2 on the surface of photocatalytic mortars nor NO oxidation took place. The concentration of NO was kept constant during the first 10 min. ii) Under UV radiation (30 min) the heterogeneous photocatalysis reaction took place and the oxidation of pollutants began – reactions (1) to (7)–. The decrease in NO concentration reached its maximum and became constant in this period of time, indicating complete activation of the TiO_2 sites. iii) During the last 10 min of the test, when the UV radiation was off, the NO concentration returned to its initial value. Contrary to what is usually observed in Portland cement-based photocatalytic mortars, the NO_2 gas profile decreased under UV radiation. This experimental observation merits additional comment further on.

Fig. 6c plots the values corresponding to removal rate (%) of NO, which is a valuable parameter to assess the specific efficiency of each mortar in the PCO. It can be observed that, in general, the higher the dosage of additive, the higher the NO abatement. Upper values of ca. 48% of NO conversion were measured for 10 wt.% TiO_2 in d-CAC, whereas the

same amount of TiO_2 in w-CAC yielded up to a 65% of abatement. The use of either type of CACs has allowed us to observe an increasing (although asymptotically) NO conversion as TiO_2 increases reaching a plateau for the maximum assayed 10 wt.% TiO_2. Conversely, in some Portland cement matrices, literature had reported that a TiO_2 upload over ca. 2 wt.% caused an inversion of the photocatalytic efficiency [32], which was interpreted as a result of the recombination between hole-pair electron in an excess of TiO_2 [33]. In the present study, the increased photocatalytic activity even for 10 wt.% of additive shows that CACs are a suitable matrix to immobilize larger amounts of photocatalytic additives when higher conversions values of NO are required. This dosage-dependence pattern is followed by CACs irrespectively of the curing regime assayed.

For a clearly quantitative comparison, we studied the initial rate constants of the NO degradation on the CAC mortars (Fig. 7). As previously reported, the initial PCO of NO followed mass transfer-controlled first-order kinetics as evidenced by the linear plot of $\ln(C/C_0)$ versus photocatalytic reaction time *t* [34,35]. The initial rate constants of the NO degradation confirmed, in a dosage-dependent pattern, the higher PCO efficiency of w-CAC samples compared with d-CAC samples (e.g.: 0.237 vs. 0.198 and 0.258 vs. 0.209 min^{-1}, respectively, for 10 wt.% TiO_2 w- and d-CAC subjected to curing condition 1 and 2) (Table 4).

The evolution of the cement compounds of the CAC matrix over time, there including the thermodynamically irreversible conversion reaction and formation of the cubic stable phases at the expense of metastable hexagonal hydrates, can be estimated from results obtained when subjecting the samples to the mild hydrothermal conditions used in curing regime 2. In this sense, the experimental results showed that the unavoidable formation of stable phases in CAC systems will not have a negative effect on the photocatalytic activity of the uploaded TiO_2, as shown by the values of the NO conversion measured in samples under both curing conditions. This effect could be also influenced by the changes in the pore structure, including an overall porosity increase due to the formation of stable hydrated aluminates.

The PCO of NO is a fast process that produces NO_2 that is partially released to the atmosphere before being fixed as nitrate ions on the mortar surface. Therefore, in order to minimize the presence of NO_x gases in the urban atmosphere it is of importance to have a good efficiency in the NO conversion but also in the NO_2 fixation. On this sense, we have paid attention to the analysis of NO_2 in the conversion chamber (Table 5) showing that CACs behave also as suitable matrices for an effective NO_2 fixation, thus contributing to a large final NO_x removal. In absolute terms, w-CAC (Fig. 6b) was more effective than d-CAC (Fig. 6a) in reducing the amount of NO_2: in 10 wt.% TiO_2-bearing samples cured under condition 1, w-CAC reduced the amount of NO_2 twice as much as d-CAC sample. Threefold NO_2 amount was removed by 10 wt.% of TiO_2 w-CAC samples in comparison with the value obtained for d-CAC samples, subjected to curing condition 2. As shown in Table 5, the percentage contribution of the NO_2 conversion to the total percentage of NO_x removal was commonly higher in w-CAC than in d-CAC samples.

This finding differs from several previous works dealing with the NO_x abatement in Portland cement-based systems. Even though the strong decomposition of NO_2 by TiO_2 photocatalytic based compounds is well known [36,37], in the case of PC samples, an increase of the NO_2 concentration is usually reported as a consequence of the fast photochemical oxidation of NO [7,9,10,38]. Although the main part of this NO_2 formed is expected to be later oxidized to nitrate ions, the amount of NO_2 evolved and not oxidized could be significant. The release of NO_2 by PC-TiO_2 systems worsens the photocalytic efficiency considering the NO_x abatement as the sum NO + NO_2. In the present study, the good efficiency of NO_2 sorption and ulterior conversion [39] can be explained by the chemical composition of the cementitious matrix of the CACs: the presence of aluminates allowed a high rate of NO_2 sorption and subsequent photooxidation, resulting in good NO_2 removal values. Although further studies will be necessary to fully elucidate the exact mechanism, the experimental fact that NO_2 decreased upon UV irradiation even in the absence of TiO_2 (Table 5, values of the control samples) prompted us to hypothesize a light-assisted mechanism, in which the UV illumination

generated holes on calcium aluminates that would act as Lewis acid sites to preferentially interact with the Lewis base NO_2. A similar interaction was described as a photoadsorption plus reaction mechanism in other photocatalytic systems [39,40]. Our proposed mechanism is consistent with (i) the experimental finding of significant NO and NO_2 abatements by plain (TiO_2-free) CACs; (ii) the improvement in these abatements in the presence of increasing amounts of TiO_2 (Table 5) showing an additional effect; (iii) existing literature that had shown that alkaline-earth metal oxides (CaO, MgO and BaO), some barium aluminates [41-44], and calcium aluminates [45] are materials with NO_2 sorption abilities, which are useful for the NO_2 removal; and (iv) the use of several divalent metal aluminates (e.g. $MgAl_2O_4$ and $ZnAl_2O_4$), structurally similar to calcium aluminates, as wide band-gap semiconductors sensitive to UV illumination [46-48].

The differences in the bulk NO_2 conversion (Table 5) observed between the plain samples of w-CAC and d-CAC can be ascribed to their diverse chemical composition: the lower amount of calcium aluminates of d-CAC in comparison with w-CAC accounts for the lower NO_2 degradation capacity measured for d-CAC.

The distinct performance between d-CAC and w-CAC is one of the factors explaining the better overall NO removal of w-CAC samples doped with TiO_2 (Fig. 6c). At the same time, as proved in the previous section, the partial interaction in d-CAC between ferrite phase and TiO_2 gave rise to iron titanates (mainly pseudobrookite and, to a lesser amount, ilmenite). This fact also contributes to explain the lower efficiency of d-CAC in the NO conversion under UV irradiation, as a consequence of the more reduced band-gaps and lower PCO activity of the resulting pseudobrookite [49-51] (2.18 eV) and ilmenite [52] (2.58 eV) in comparison with a band-gap of 3.2 eV for TiO_2, together with a reduction of active sites of the titania surface [53]. A certain amount of unreacted TiO_2 still observed in doped d-CAC samples (Fig. 3) also contributed to the NO conversion of these samples.

Overall, thanks to the good efficiency in the NO and NO_2 conversion, the CAC-based mortars exhibited a very remarkable NO_x removal rate (Table 6). Best values were obtained for w-CAC samples, the NO_x conversion reaching an outstanding value (60.4%). Comparatively, under similar experimental conditions, a NO_x conversion lower than 28% was reported for Portland cement-based pastes with 3.5% of TiO_2 [5]. This feature guarantee the effectiveness of TiO_2-modified CACs as depolluting materials to be used in many practical applications in which CACs are applied, such as tunnels, industrial floors and urban areas.

4. Conclusions

Calcium aluminate cements, modified by incorporation of different percentages of TiO_2, have been successfully identified as depolluting materials for NOx reduction. The TiO_2 presence rendered doped mortars with significant compressive strengths over 20 MPa.

An iron-rich (d-CAC) and an iron-lean (w-CAC) calcium aluminate cements have been tested. The ferrite (brownmillerite) phase present in the d-CAC was found to be responsible for the occurrence of an interaction with the TiO_2 added, involving the development of certain amounts of iron titanates, mainly pseudobrookite.

NO conversion rates ca. 48% and 65% were measured, respectively, for 10 wt.% TiO_2 d-CAC and w-CAC mortars. The behaviour of the d-CAC mortars is partially ascribable to the presence of iron titanates with a smaller band-gap than that of TiO_2.

The good PCO performance even for samples containing 10 wt. % of additive proved these CAC matrices suitable to immobilize large amounts of photocatalytic additives when higher conversions values of NO are required.

Samples cured under the hydrothermal curing condition 2 that forced the conversion of metastable hydrates into stable cubic phases maintained the photocatalytic efficiency. This finding suggests a long-term PCO activity of this type of cementitious systems.

Thanks to the presence of calcium aluminates, these materials were found to be good sorbent agents for NO_2 as compared with other binding matrices, thus improving the overall NO_x abatement rate achieved.

Acknowledgements

The authors want to thank Ciments Molins and Kerneos España for the material supplied. They also acknowledge Dr. E. Baquero for the SEM analysis. This work was funded by Fundación Universitaria de Navarra (grant FUNA2013-15108402); by Junta de Andalucía (Group FQM-175 and P09-FQM-174 Project from Consejería de Innovación, Ciencia y Empresa) and by the European Union (FEDER Andalucía 2007-13). M. Pérez-Nicolás thanks the Friends of the University of Navarra, Inc., for a pre-doctoral grant.

References

[1] Beevers, S.D.; Westmoreland, E.; de Jong, M.C.; Williams, M.L.; Carslaw, D.C. Trends in NO_x and NO_2 emissions from road traffic in Great Britain. *Atmos. Environ.* **2012,** *54* (0), 107-116; DOI: 10.1016/j.atmosenv.2012.02.028.

[2] Manahan, S.E. *Environmental Chemistry.* CRC Press: 2005; pp 310.

[3] Di Paola, A.; García-López, E.; Marcì, G.; Palmisano, L. A survey of photocatalytic materials for environmental remediation. *J. Hazard. Mater.* **2012,** *211–212* (0), 3-29; DOI: 10.1016/j.jhazmat.2011.11.050.

[4] Chen, J.; Kou, S.; Poon, C. Photocatalytic cement-based materials: Comparison of nitrogen oxides and toluene removal potentials and evaluation of self-cleaning performance. *Build. Environ.* **2011,** *46* (9), 1827-1833; DOI: 10.1016/j.buildenv.2011.03.004.

[5] Folli, A.; Pade, C.; Hansen, T.B.; De Marco, T.; Macphee, D.E. TiO_2 photocatalysis in cementitious systems: Insights into self-cleaning and depollution chemistry. *Cem. Concr. Res.* **2012,** *42* (3), 539-548; DOI: 10.1016/j.cemconres.2011.12.001.

[6] Smits, M.; Huygh, D.; Craeye, B.; Lenaerts, S. Effect of process parameters on the photocatalytic soot degradation on self-cleaning cementitious materials. *Catal. Today* **2014,** *In Press, Corrected Proof*; DOI: 10.1016/j.cattod.2013.10.001.

[7] Sugrañez, R.; Álvarez, J.I.; Cruz-Yusta, M.; Mármol, I.; Morales, J.; Vila, J.; Sánchez, L. Enhanced photocatalytic degradation of NO_x gases by regulating the microstructure of mortar cement modified with titanium dioxide. *Build. Environ.* **2013,** *69* (0), 55-63; DOI: 10.1016/j.buildenv.2013.07.014.

[8] Ibusuki, T. Cleaning Atmospheric Environment (Photocatalytic activities of TiO_2), In *Photocatalysis: Science and Technology,* Kaneko, M. and Okura, I., Eds.; Springer: Berlin Heidelberg, 2010; pp. 143.

[9] Chen, J. and Poon, C. Photocatalytic Cementitious Materials: Influence of the Microstructure of Cement Paste on Photocatalytic Pollution Degradation. *Environ. Sci. Technol.* **2009,** *43* (23), 8948-8952; DOI: 10.1021/es902359s.

[10] Cárdenas, C.; Tobón, J.I.; García, C.; Vila, J. Functionalized building materials: Photocatalytic abatement of NO_x by cement pastes blended with TiO_2 nanoparticles. *Constr. Build. Mater.* **2012,** *36* (0), 820-825; DOI: 10.1016/j.conbuildmat.2012.06.017.

[11] Klaus, S.R.; Neubauer, J.; Goetz-Neunhoeffer, F. Hydration kinetics of CA2 and CA—Investigations performed on a synthetic calcium aluminate cement. Cem. Concr. Res. 2013, 43, 62-69.

[12] Ukrainczyk, N.; Vrbos, N.; Šipušić, J. Influence of metal chloride salts on calcium aluminate cement hydration. *Adv. Cem. Res.* **2012,** *24* (5), 249-262; DOI: 10.1680/adcr.11.00012.

[13] Juenger, M.C.G.; Winnefeld, F.; Provis, J.L.; Ideker, J.H. Advances in alternative cementitious binders. *Cem. Concr. Res.* **2011,** *41* (12), 1232-1243; DOI: 10.1016/j.cemconres.2010.11.012.

[14] Scrivener, K.L. and Capmas, A. Calcium Aluminate Cements, In *Lea's Chemistry of Cement and Concrete (Fourth Edition),* Hewlett, P.C., Ed.; Butterworth-Heinemann: Oxford, 2003; pp. 713-782.

[15] Navarro-Blasco, I.; Duran, A.; Sirera, R.; Fernández, J.M.; Alvarez, J.I. Solidification/stabilization of toxic metals in calcium aluminate cement matrices. *J. Hazard. Mater.* **2013,** *260* (0), 89-103; DOI: 10.1016/j.jhazmat.2013.04.048.

[16] European Committee for Standardization UNE-EN 1015-3: 2000 Methods of test for mortar for masonry. Part 3: Determination of consistence of fresh mortar (by flow table); CEN: Brussels. **2000**.

[17] European Committee for Standardization UNE-EN 1015-19: 2000 Methods of test for mortar for masonry. Part 9: Determination of workable life and correction time of fresh mortar; CEN: Brussels. **2000**.

[18] ISO 22197-1 Fine ceramics (advanced ceramics, advanced technical ceramics). Test method for air purification performance of semiconducting photocatalytic materials. Part 1: Removal of nitric oxide. **2007**.

[19] Jansen, D.; Neubauer, J.; Goetz-Neunhoeffer, F.; Haerzschel, R.; Hergeth, W.-D. Change in reaction kinetics of a Portland cement caused by a superplasticizer — Calculation of heat flow curves from XRD data. *Cem. Concr. Res.* **2012,** *42* (2), 327-332.

[20] Torréns-Martín, D.; Fernández-Carrasco, L.; Martínez-Ramírez, S. Hydration of calcium aluminates and calcium sulfoaluminate studied by Raman spectroscopy. *Cem. Concr. Res.* **2013,** *47* (0), 43-50; DOI: 10.1016/j.cemconres.2013.01.015.

[21] Emanuelson, A.; Henderson, E.; Hansen, S. Hydration of ferrite Ca_2AlFeO_5 in the presence of sulphates and bases. *Cem. Concr. Res.* **1996,** *26* (11), 1689-1694; DOI: 10.1016/S0008-8846(96)00154-8.

[22] Sant, G.; Ferraris, C.F.; Weiss, J. Rheological properties of cement pastes: A discussion of structure formation and mechanical property development. *Cem. Concr. Res.* **2008,** *38* (11), 1286-1296; DOI: 10.1016/j.cemconres.2008.06.008.

[23] Pal, B.; Sharon, M.; Nogami, G. Preparation and characterization of TiO_2/Fe_2O_3 binary mixed oxides and its photocatalytic properties. *Mater. Chem. Phys.* **1999,** *59* (3), 254-261; DOI: 10.1016/S0254-0584(99)00071-1.

[24] Ukrainczyk, N.; Matusinović, T. Thermal properties of hydrating calcium aluminate cement pastes, *Cem. Concr. Res.***2010**, 40(1),128-36, DOI: 10.1016/j.cemconres.2009.09.005.

[25] Luo, J.; Xing, X.; Yu, R.; Xing, Q.; Liu, G.; Zhang, D.; Chen, X. Low-temperature synthesis and characterization of $(Zn,Ni)TiO_3$ ceramics by a modified sol–gel route. *J. Alloys Compd.* **2006**, 420(1–2), 317-21; DOI: 10.1016/j.jallcom.2005.10.050.

[26] Vinogradov, A.V.; Vinogradov, V.V.; Gerasimova, T.V.; Agafonov, A.V. Low-temperature sol–gel synthesis of nanosized pseudobrookite crystals without heat treatment. *J. Alloys Compd.* **2012**, 535, 102-7; DOI: 10.1016/j.jallcom.2012.04.066.

[27] Vinogradov, A.V.; Vinogradov, V.V.; Gerasimova, T.V.; Agafonov, A.V. Low-temperature sol–gel synthesis of crystalline $CoTiO_3$ coatings without annealing. *J. Alloys Compd.* **2012,** 543, 172-5; DOI: 10.1016/j.jallcom.2012.06.102.

[28] Suttiponparnit, K.; Jiang, J.; Sahu, M.; Suvachittanont, S.; Charinpanitkul, T.; Biswas, P. Role of surface area, primary particle size, and crystal phase on titanium dioxide nanoparticle dispersion properties. *Nanoscale Res. Lett.* **2011**, 6 (27), 1-8.

[29] Lackhoff, M.; Prieto, X.; Nestle, N.; Dehn, F.; Niessner, R. Photocatalytic activity of semiconductor-modified cement—influence of semiconductor type and cement ageing. *Appl. Catal. , B* **2003,** *43* (3), 205-216; DOI: 10.1016/S0926-3373(02)00303-X.

[30] Navarro-Blasco, Í; Fernández, J.M.; Duran, A.; Sirera, R.; Álvarez, J.I. A novel use of calcium aluminate cements for recycling waste foundry sand (WFS). *Constr. Build. Mater.* **2013,** *48* (0), 218-228; DOI: 10.1016/j.conbuildmat.2013.06.071.

[31] Morejón-Alonso, L.; García Carrodeguas, R.; dos Santos, L.A. Development and characterization of α-tricalcium phosphate/monocalcium aluminate composite bone cement. *J. Biomedical Science and Engineering* **2012,** *5*, 448-456; DOI: 10.4236/jbise.2012.58057.

[32] Lucas, S.S.; Ferreira, V.M.; de Aguiar, J.L.B. Incorporation of titanium dioxide nanoparticles in mortars — Influence of microstructure in the hardened state properties and photocatalytic activity. *Cem. Concr. Res.* **2013,** *43* (0), 112-120; DOI: 10.1016/j.cemconres.2012.09.007.

[33] Carp, O.; Huisman, C.L.; Reller, A. Photoinduced reactivity of titanium dioxide. *Prog. Solid State Chem.* **2004,** *32* (1–2), 33-177; DOI: 10.1016/j.progsolidstchem.2004.08.001.

[34] Ai, Z.; Ho, W.; Lee, S.; Zhang, L. Efficient Photocatalytic Removal of NO in Indoor Air with Hierarchical Bismuth Oxybromide Nanoplate Microspheres under Visible Light. *Environ. Sci. Technol.* **2009,** *43* (11), 4143-4150; DOI: 10.1021/es9004366.

[35] Ai, Z.; Zhang, L.; Lee, S. Efficient Visible Light Photocatalytic Oxidation of NO on Aerosol Flow-Synthesized Nanocrystalline $InVO_4$ Hollow Microspheres. *J. Phys. Chem., C* **2010,** *114* (43), 18594-18600; DOI: 10.1021/jp106906s.

[36] Monge, M.E.; D'Anna, B.; George, C. Nitrogen dioxide removal and nitrous acid formation on titanium oxide surfaces-an air quality remediation process? *Phys.Chem.Chem.Phys.* **2010,** *12* (31), 8991-8998; DOI: 10.1039/B925785C.

[37] Laufs, S.; Burgeth, G.; Duttlinger, W.; Kurtenbach, R.; Maban, M.; Thomas, C.; Wiesen, P.; Kleffmann, J. Conversion of nitrogen oxides on commercial photocatalytic dispersion paints. *Atmos. Environ.* **2010,** *44* (19), 2341-2349; DOI: 10.1016/j.atmosenv.2010.03.038.

[38] Martinez, T.; Bertron, A.; Ringot, E.; Escadeillas, G. Degradation of NO using photocatalytic coatings applied to different substrates. *Build. Environ.* **2011,** *46* (9), 1808-1816; DOI: 10.1016/j.buildenv.2011.03.001.

[39] Folli, A.; Campbell, S.B.; Anderson, J.A.; Macphee, D.E. Role of TiO_2 surface hydration on NO oxidation photo-activity. *J. Photochem. Photobiol. A.* **2011,** *220* (2–3), 85-93; DOI: 10.1016/j.jphotochem.2011.03.017.

[40] Devahasdin, S.; Fan Jr., C.; Li, K.; Chen, D.H. TiO2 photocatalytic oxidation of nitric oxide: transient behavior and reaction kinetics. *J. Photochem. Photobiol. A.* **2003,** *156* (1–3), 161-170; DOI: 10.1016/S1010-6030(03)00005-4.

[41] Hodjati, S.; Vaezzadeh, K.; Petit, C.; Pitchon, V.; Kiennemann, A. NO_x sorption–desorption study: application to diesel and lean-burn exhaust gas (selective NOx recirculation technique). *Catal. Today* **2000,** *59* (3–4), 323-334; DOI: 10.1016/S0920-5861(00)00298-4.

[42] Hodjati, S.; Bernhardt, P.; Petit, C.; Pitchon, V.; Kiennemann, A. Removal of NO_x: Part I. Sorption/desorption processes on barium aluminate. *Appl. Catal. , B* **1998,** *19* (3–4), 209-219; DOI: 10.1016/S0926-3373(98)00077-0.

[43] Hodjati, S.; Bernhardt, P.; Petit, C.; Pitchon, V.; Kiennemann, A. Removal of NO_x: Part II. Species formed during the sorption/desorption processes on barium aluminates. *Appl. Catal. , B* **1998,** *19* (3–4), 221-232; DOI: 10.1016/S0926-3373(98)00086-1.

[44] Akiti Jr., T.T.; Constant, K.P.; Doraiswamy, L.K.; Wheelock, T.D. Development of an advanced calcium-based sorbent for desulfurizing hot coal gas. *Adv. Environ. Res.* **2001,** *5* (1), 31-38; DOI: 10.1016/S1093-0191(00)00039-3.

[45] Proto, A.; Cucciniello, R.; Rossi, F.; Motta, O. Ca-based adsorbents for NO_x measurement in atmospheric environments surrounding monumental and archeological sites, In *Built Heritage 2013 Monitoring Conservation Management,* Boriani, M., Gabaglio, R. and Gulotta, D., Eds.; Politecnico di Milano, Centro per la Conservazione e Valorizzazione dei Beni Culturali: Milano, 2013; pp. 1447.

[46] Ragupathi, C.; Vijaya, J.J.; Narayanan, S.; Kennedy, L.J.; Ramakrishna, S. Catalytic properties of nanosized zinc aluminates prepared by green process using Opuntia dilenii haw

plant extract. *Chin. J. Catal.* **2013,** *34* (10), 1951-1958; DOI: 10.1016/S1872-2067(12)60682-2.

[47] Song, J.; Leng, M.; Fu, X.; Liu, J. Synthesis and characterization of nanosized zinc aluminate spinel from a novel Zn–Al layered double hydroxide precursor. *J. Alloys Compounds* **2012,** *543* (0), 142-146; DOI:10.1016/j.jallcom.2012.07.111.

[48] Tabaza, W.A.I.; Swart, H.C.; Kroon, R.E. Luminescence of Ce doped $MgAl_2O_4$ prepared by the combustion method. *Physica B* **2014,** *439* (0), 109-114; DOI: 10.1016/j.physb.2013.10.060.

[49] Ye, F.X.; Tsumura, T.; Nakata, K.; Ohmori, A. Dependence of photocatalytic activity on the compositions and photo-absorption of functional TiO_2–Fe_3O_4 coatings deposited by plasma spray. *Mater. Sci. Eng. , B* **2008,** *148* (1–3), 154-161; DOI: 10.1016/j.mseb.2007.09.057.

[50] Smith, Y.R.; Joseph Antony Raj, K.; (Ravi) Subramanian, V.; Viswanathan, B. Sulfated Fe_2O_3–TiO_2 synthesized from ilmenite ore: A visible light active photocatalyst. *Colloids Surf. Physicochem. Eng. Aspects* **2010,** *367* (1–3), 140-147; DOI: 10.1016/j.colsurfa.2010.07.001.

[51] Litter, M.I. and Navío, J.A. Photocatalytic properties of iron-doped titania semiconductors. *J. Photochem. Photobiol. A.* **1996,** *98* (3), 171-181; DOI: 10.1016/1010-6030(96)04343-2.

[52] Ye, F. and Ohmori, A. The photocatalytic activity and photo-absorption of plasma sprayed TiO_2–Fe_3O_4 binary oxide coatings. *Surf. Coat. Technol.* **2002,** *160* (1), 62-67; DOI: 10.1016/S0257-8972(02)00377-8.

[53] Fàbrega, C.; Andreu, T.; Cabot, A.; Morante, J.R. Location and catalytic role of iron species in TiO_2:Fe photocatalysts: An EPR study. *J. Photochem. Photobiol. A.* **2010,** *211* (2–3), 170-175; DOI: 10.1016/j.jphotochem.2010.03.003.

Table 1. Chemical and mineralogical composition of the iron-rich, dark-CAC and white-CAC

Cement	***Al_2O_3 (%)***	***CaO (%)***	***Fe_2O_3 (%)***	***SiO_2 (%)***	***SO_3 (%)***	***Na_2O+K_2O (%)***	***Main mineralogical phases***	***Minor mineralogical phases***
d-CAC	42.0	37.8	17.0	3.0	0.1	0.1	$CaAl_2O_4$ (CA)	Ca_2FeAlO_5 (C_4AF), $Ca_{12}Al_{14}O_{33}$ ($C_{12}A_7$), ß-Ca_2SiO_4 (C_2S), $Ca_3TiFe_2O_8$, FeO
w-CAC	70.9	28.0	0.1	0.2	<0.3	<0.5	$CaAl_2O_4$, (CA), $CaAl_4O_8$ (CA_2)	$Ca_{12}Al_{14}O_{33}$ ($C_{12}A_7$)

Table 2. Percentages of superplasticizer added and setting time values of the different mortars.

Cement type	*% TiO_2*	*Superplasticizer (%)*	*Setting time (min)*
d-CAC	0	0.07	15
	1	0.20	17
	3	0.40	26
	5	1.30	32
	10	2.50	115
w-CAC	0	0.10	5
	1	0.20	11
	3	0.40	20
	5	0.60	18
	10	1.10	21

Table 3. XRD results of the tested samples.

Mineralogical phase	*Control d-CAC*		*5% TiO_2 d-CAC*		*10% TiO_2 d-CAC*		*Control w-CAC*		*5% TiO_2 w-CAC*		*10% TiO_2 w-CAC*	
	Curing		*Curing*		*Curing*		*Curing*		*Curing*		*Curing*	
	1	*2*	*1*	*2*	*1*	*2*	*1*	*2*	*1*	*2*	*1*	*2*
SiO_2 (quartz)	**	**	**	**	**	**	**	**	**	**	**	**
CA ($CaAl_2O_4$)	*	s	t	t	t	t	s	t	t	t	t	t
$C_{12}A_7$ (mayenite)	*	-	s	-	s	-	*	-	s	-	s	-
CAH_{10} ($CaAl_2O_4.10H_2O$)	**	*	*	s	*	s	*	s	*	s	*	s
C_2AH_8 ($Ca_2Al_2O_5.8H_2O$)	*	s	*	s	*	s	*	s	*	s	*	s
AH_3 (gibbsite)	-	s	-	*	-	*	-	*	-	*	-	*
C_3AH_6 (hydrogarnet)	-	*	-	*	-	*	-	*	-	*	-	*
C_4AF (brownmillerite)	*	s	-	-	-	-	-	-	-	-	-	-
TiO_2 (anatase)	-	-	t	t	t	t	-	-	*	*	*	*
$FeTiO_3$ (ilmenite)	-	-	t	t	t	t	-	-	-	-	-	-
$FeTi_2O_5$ (pseudobrookite)	-	-	s	t	s	t	-	-	-	-	-	-

**: Very intense diffraction peaks
*: intense diffraction peaks
s: small diffraction peaks
t: traces
-: not detected

Table 4. Initial rate constants of the NO degradation over d-CAC and w-CAC samples subjected at different curing conditions.

Curing condition 1	***K (min^{-1})***	***Curing condition 2***	***K (min^{-1})***
d-CAC 0% TiO_2	0.017	*d-CAC 0% TiO_2*	0.016
d-CAC 1% TiO_2	0.140	*d-CAC 1% TiO_2*	0.139
d-CAC 3% TiO_2	0.085	*d-CAC 3% TiO_2*	0.156
d-CAC 5% TiO_2	0.176	*d-CAC 5% TiO_2*	0.210
d-CAC 10% TiO_2	0.198	*d-CAC 10% TiO_2*	0.209
w-CAC 0% TiO_2	0.018	*w-CAC 0% TiO_2*	0.054
w-CAC 1% TiO_2	0.122	*w-CAC 1% TiO_2*	0.202
w-CAC 3% TiO_2	0.106	*w-CAC 3% TiO_2*	0.242
w-CAC 5% TiO_2	0.241	*w-CAC 5% TiO_2*	0.298
w-CAC 10% TiO_2	0.237	*w-CAC 10% TiO_2*	0.258

Table 5. Conversion values of nitrogen oxides by the assayed mortars (ppbv).

Curing condition 1									
d-CAC	***NO***	***NO_2***	***NO_x***	***NO_2/NO_x****	***w-CAC***	***NO***	***NO_2***	***NO_x***	***NO_2/NO_x****
Control	161.3	21.3	182.6	11.7	*Control*	137.8	48.5	186.3	26.1
1%	389.4	51.7	441.2	11.7	*1%*	400.8	62.7	463.5	13.5
3%	247.8	39.1	286.8	13.6	*3%*	485.3	64.1	549.5	11.7
5%	438.3	30.1	468.3	6.4	*5%*	543.4	92.8	636.2	14.6
10%	476.7	39.6	516.3	7.7	*10%*	555.1	80.3	635.3	12.6
Curing condition 2									
d-CAC	***NO***	***NO_2***	***NO_x***	***NO_2/NO_x****	***w-CAC***	***NO***	***NO_2***	***NO_x***	***NO_2/NO_x****
Control	112.8	22.5	135.3	16.7	*Control*	178.5	37.4	215.9	17.3
1%	355.9	33.3	389.2	8.6	*1%*	477.3	38.8	516.1	7.5
3%	416.3	13.6	429.9	3.2	*3%*	521.3	60.8	582.0	10.4
5%	452.3	23.6	475.9	5.0	*5%*	623.2	73.5	696.7	10.6
10%	486.3	31.4	517.6	6.1	*10%*	646.8	102.7	749.5	13.7

* Contribution ratio (%) of NO_2 abatement to total NO_x degradation

Table 6. The NO_x removal rate (%) obtained for d-CAC and w-CAC samples with different TiO_2 content and subjected at different curing conditions.

Curing condition 1	***NO_x removal (%)***	***Curing condition 2***	***NO_x removal (%)***
d-CAC 0% TiO_2	17.05	*d-CAC 0% TiO_2*	11.90
d-CAC 1% TiO_2	40.08	*d-CAC 1% TiO_2*	33.68
d-CAC 3% TiO_2	26.08	*d-CAC 3% TiO_2*	37.52
d-CAC 5% TiO_2	43.10	*d-CAC 5% TiO_2*	41.82
d-CAC 10% TiO_2	47.67	*d-CAC 10% TiO_2*	45.55
w-CAC 0% TiO_2	14.97	*w-CAC 0% TiO_2*	17.23
w-CAC 1% TiO_2	37.57	*w-CAC 1% TiO_2*	41.52
w-CAC 3% TiO_2	44.81	*w-CAC 3% TiO_2*	46.76
w-CAC 5% TiO_2	51.08	*w-CAC 5% TiO_2*	56.87
w-CAC 10% TiO_2	51.47	*w-CAC 10% TiO_2*	60.40

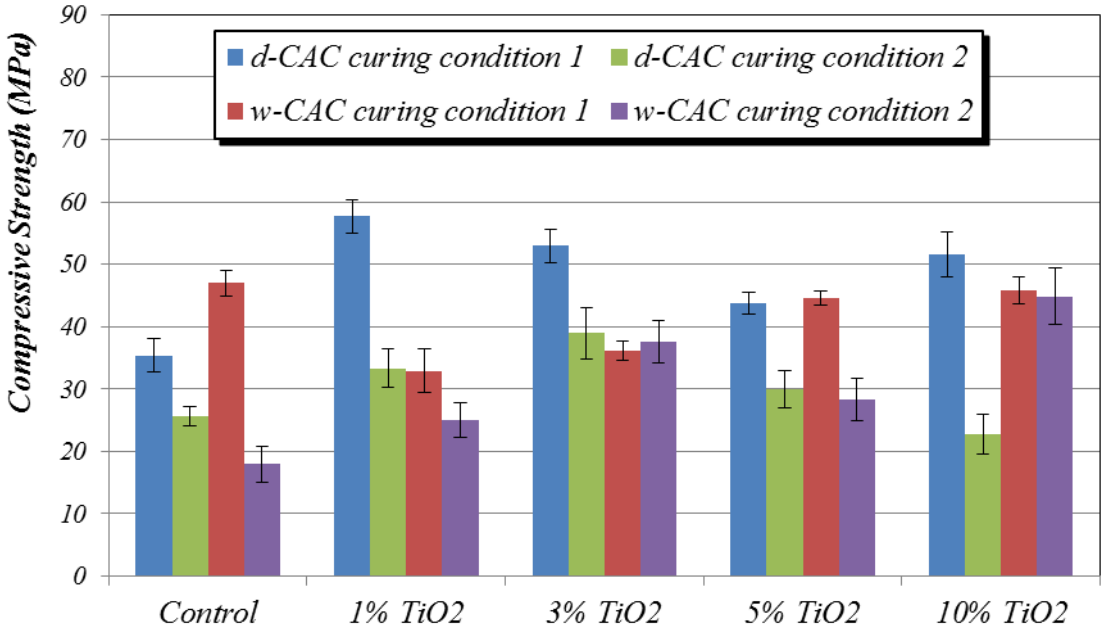

Figure 1. Compressive strength values of d- and w-CAC mortars doped with TiO_2 under curing conditions 1 and 2.

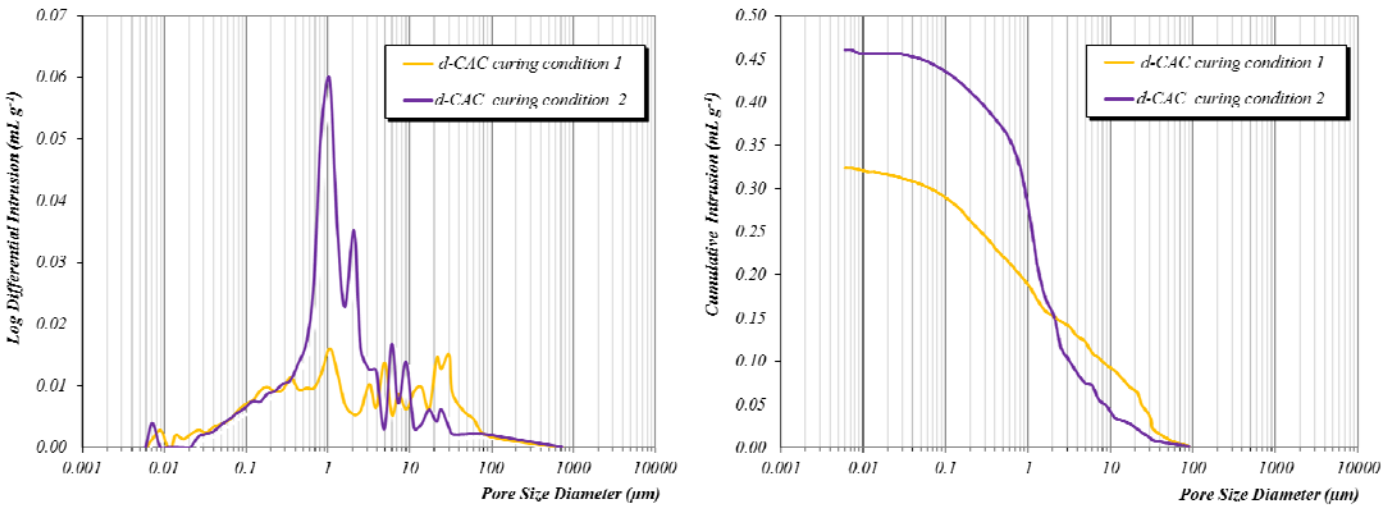

Figure 2. Pore size distributions of TiO_2-free d-CAC samples cured under the two different conditions: differential intrusion curves (left) and cumulative intrusion curves (right).

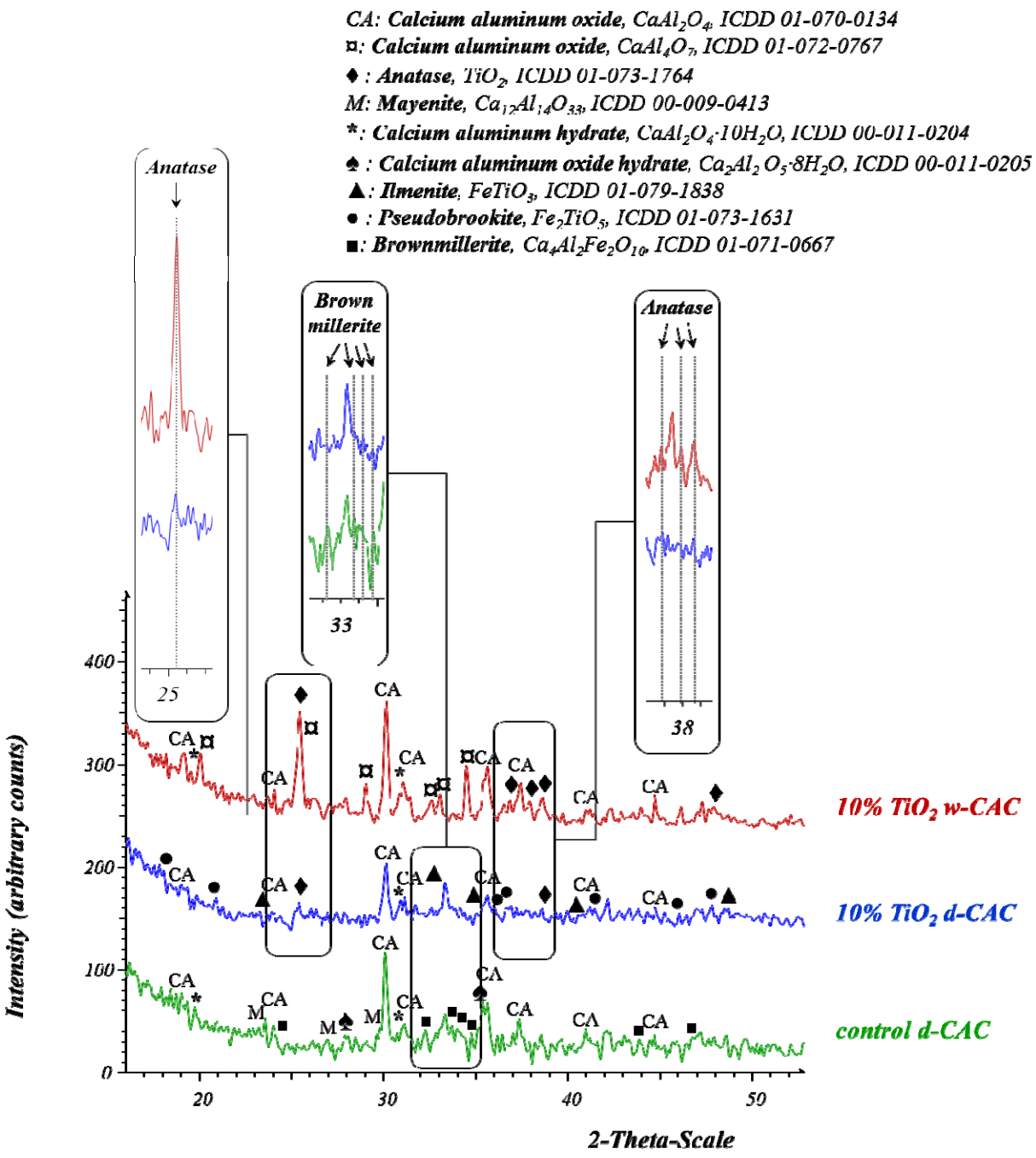

Figure 3. XRD patterns of different CAC pastes.

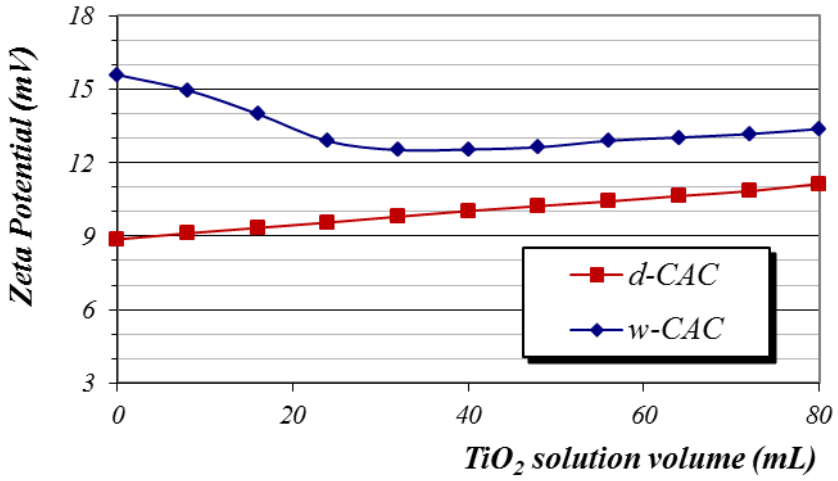

Figure 4. Zeta potential values of d- and w-CAC suspensions titrated with a solution of 0.5 wt. % TiO_2.

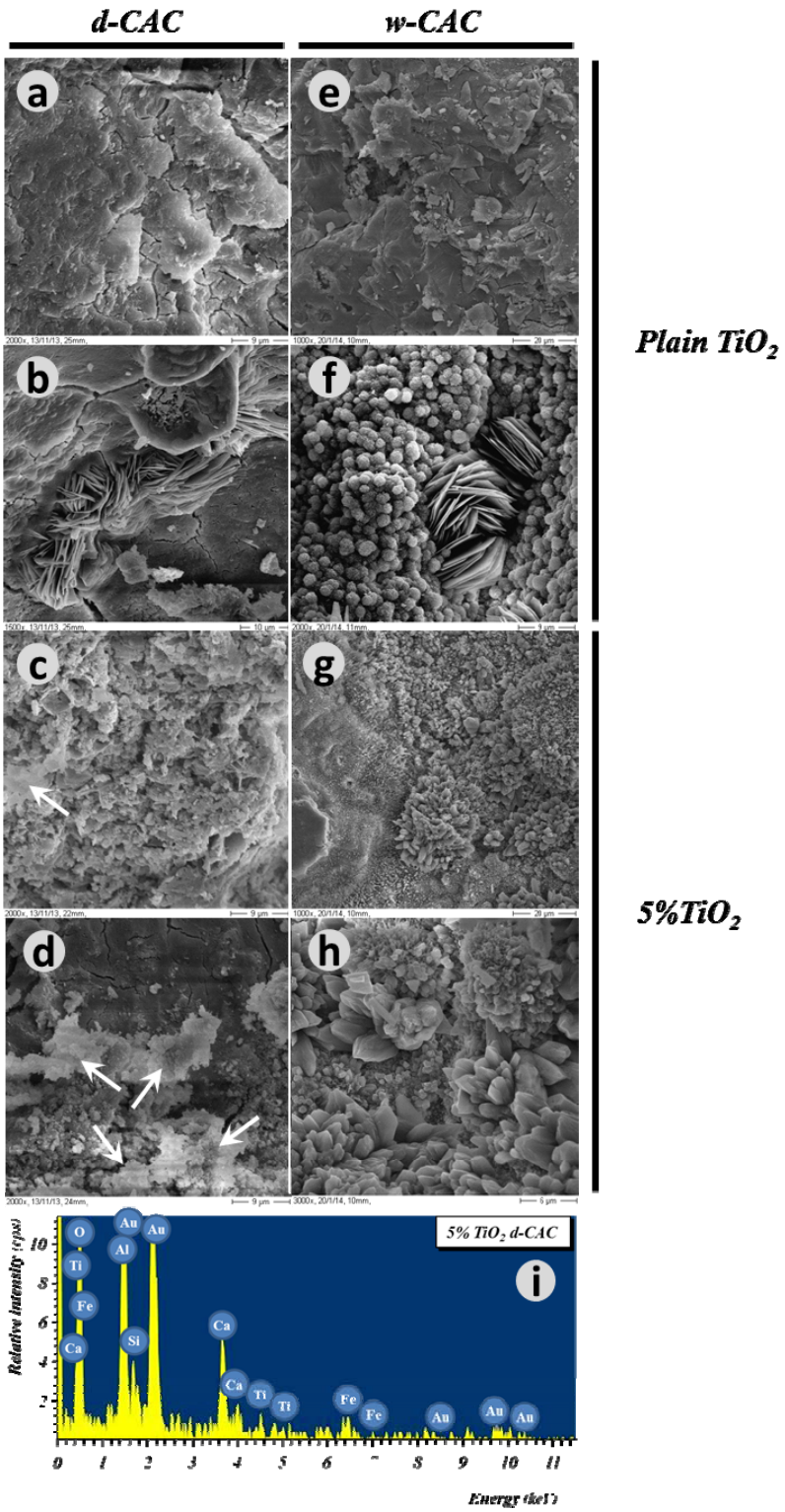

Figure 5. SEM micrographs of CAC samples after curing condition 1. Samples of d-CAC are depicted on the left part; w-CAC samples appear on the right side. a), b), e) and f) micrographs of plain (TiO_2-free) samples. c), d), g) and h) correspond with 5 wt.% TiO_2 samples. i) EDAX analysis of a spot of a TiO_2-bearing d-CAC sample.

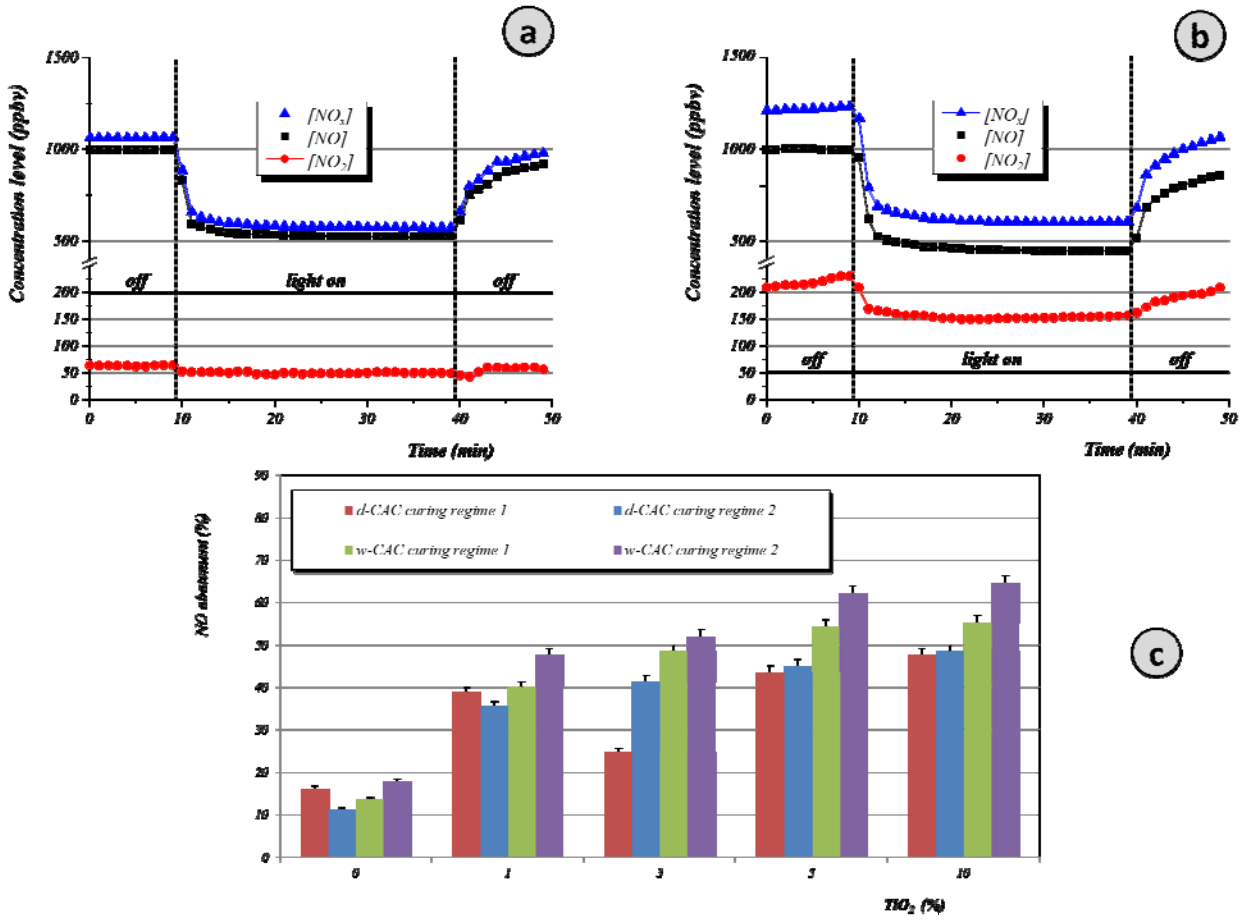

Figure 6. Profiles of NO, NO_2 and NO_x abatements for d-CAC (a) and w-CAC (b) samples loaded with 10 wt.% TiO_2; c) Percentages of NO abatement for all the samples assayed.

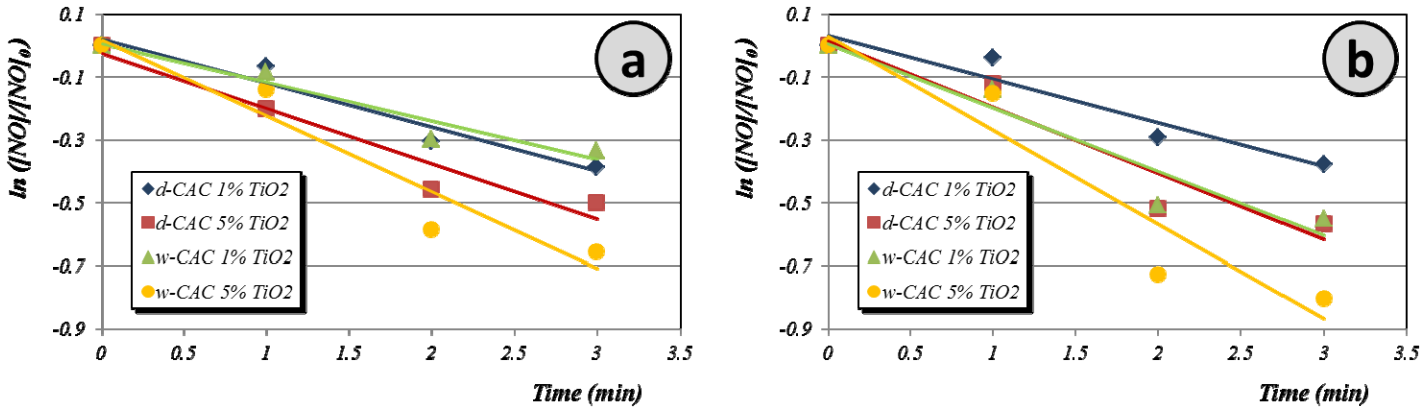

Figure 7. Dependence of $\ln([NO]/[NO]_0)$ on irradiation time under UV light for d- and w-CAC samples after (a) curing condition 1 and (b) curing condition 2.